Available online at www.sciencedirect.com
SCIENCE DIRECT®
Journal of Nuclear Materials 321 (2003) 324–330
journal of nuclear materials
www.elsevier.com/locate/jnucmat

Behaviour of fission gases in an irradiated nuclear fuel under α external irradiation

L. Desgranges [a,*], M. Ripert [b,1], J.P. Piron [b,1], H. Kodja [c,2], J.P. Gallier [c,2]

[a] CEA Cadarache, DEN/DEC/S3C/LECMI, Bât. 316, 13108 St Paul Lez Durance, France
[b] CEA Cadarache, DEN/DEC/SESC, Bât. 315, 13108 Saint Paul Lez Durance, France
[c] CEA Saclay, DSM/DRECAM/LPS, Bât. 637, 91191 Gif sur Yvette, France

Received 10 March 2003; accepted 12 June 2003

Abstract

The self-α-irradiation could influence the behaviour of nuclear spent fuel in storage conditions. To evaluate some of these effects, a UO_2 fuel, irradiated in a PWR, was irradiated with a helium beam at different doses. PIXE measurements of xenon and neodymium concentration on helium irradiated and non-irradiated areas showed that no major difference in the distribution of these fission products occurred due to helium irradiation. From these results, it is concluded that helium irradiation associated with α self-irradiation does not induce significant modification of gaseous fission products in storage conditions.

PACS: 81.05.JE; 28.41.Bm

1. Introduction

The study of the behaviour of irradiated fuel, either uranium oxide (UOX) or Uranium, Plutonium mixed oxide (MOX), during interim storage is an active field of research in France nowadays [1]. Due to the lack of nuclear fuel stored for sufficiently long periods of time, a simulation strategy has been adopted to determine how irradiated fuel could evolve over long periods of time. This simulation cannot involve only computational modelling because this would mean that all phenomena occurring in the irradiated fuel are known, understood and described by equations, which is far from the present state of our knowledge. For example, many questions remain unsolved concerning the evolution of irradiated fuel at low temperature and the diffusion enhanced by α irradiation, two issues of particular interest for interim storage.

Fuel placed in interim storage will operate at a temperature lower (less than 300 °C for most of the duration of the storage) than that of a PWR irradiation (from 500 °C at periphery to 1000–1200 °C at the pellet centre). The behaviour of the fuel could change according to temperature such as the $MgAl_2O_4$ ceramics which is stable at high temperature and swells at low temperature due to the build-up of defects. The recovery temperature of these defects is too high to allow the restoration of the crystal lattice at low temperature [2]. In unirradiated UO_2, the temperature for the recovery of several atomic defects was estimated. All atomic defects are restored for temperatures higher than 700–800 °C [3]. This clearly means that the defects produced during (interim) storage will partly accumulate, while most of them are recovered during in-pile irradiation. Although the behaviour of the unit cell parameter of non-irradiated fuel under self-α-irradiation was proved to saturate after some accumulation of damage [4], much less is known about the behaviour of irradiated fuel.

* Corresponding author. Tel.: +33-4 4225 3159; fax: +33-4 4225 3611.
E-mail address: ldesgranges@cea.fr (L. Desgranges).
[1] Tel.: +33-4 4225 7041; fax: +33-4 4225 4747.
[2] Tel.: +33-1 6908 6496; fax: +33-1 6908 6923.

0022-3115/$ - see front matter
doi:10.1016/S0022-3115(03)00304-0

Moreover, even during in-reactor operation, the colder part (approximately 500 °C) of the fuel in the outer edge of the pellet exhibits the so-called "rim effect" or high burn-up structure (HBS). During irradiation the capture of epithermal neutrons induces indeed a burn-up increase at the pellet edge. The concentration of fission products measured with EPMA is correlatively increased except for rare gases. Due to the formation of bubbles, the xenon intensity measured with EPMA decreases abruptly over a threshold burn-up [5]. The HBS is also characterised by the appearance of this fine porosity and the transformation of initial 10 μm grains in submicron subgrains [6]. It is generally agreed that the HBS formation can be attributed to the accumulation of irradiation damage but the precise mechanism is still under discussion [7–10]. It is therefore justifiable to wonder if some part of the irradiated fuel might undergo transformation into HBS due to its residual internal irradiation during interim storage.

Irradiation-enhanced diffusion is indeed considered to play a major role for temperatures below 1000 °C during in-pile irradiation [3]. It results from the effect of the fission recoil on the diffusion of fission products. The phenomenological coefficient of this effect has been derived but exact description of the phenomenon is very complex including direct recoil and vacancy creation.

Under storage conditions, α disintegration is the main source of damage for the nuclear ceramic. Fast neutron emission and spontaneous fission density are indeed six orders of magnitude lower than the α activity in storage conditions [11] while the beta decay from fission products and few actinides (i.e. ^{241}Pu) induces only a very low recoil energy of the emitting atom, lower than the minimum displacement energy [12]. The α irradiation dose in storage conditions was evaluated on the basis of neutron physics calculations [13]. For a UO_2 fuel at 47.5 GWd/tU, the α dose would be 4.7×10^{18} He at./cm^3 after 3 years of storage and 3.3×10^{19} He at./cm^3 after 300 years of storage. For a MOX fuel with the same burn-up, the α dose would be 3.6×10^{19} He at./cm^3 after 3 years of storage and 2.2×10^{20} He at./cm^3 after 300 years of storage. Moreover in MOX fuel, this α dose is not distributed homogeneously but is enhanced in the plutonium-enriched agglomerates in which the concentration of α emitters is higher.

α self-irradiation combines the effects of the two particles emitted during disintegration: a heavy recoil atom and an $^4He^{2+}$ ion. The recoil atom has an energy of 0.1 MeV and produces around 1500 Frenkel pairs along the stopping distance within a range of 10–20 nm. The α particle has an energy of 5.5 MeV and produces 100–200 Frenkel pairs at the end of a 12 μm distance. Most of the energy is dissipated by ionisation of the lattice atoms along the track of the α particle [14]. It is thus assumed that the α disintegration damage in the crystal is mainly induced by the recoil atoms. However the influence of the α particles should not be underestimated because, in the case of a MOX stored 300 years, they produce approximatively one Frenkel pair for each actinide atom.

We shall focus here on the influence of α particle on xenon mobility in irradiated UO_2 fuel. The purpose of this paper is to check experimentally that damage due to an irradiation by α particles does not significantly modify the location of xenon in the lattice of a high burn-up UO_2 fuel. An irradiated fuel sample is submitted to an irradiation similar to one it would undergo during interim storage. In this experimental simulation, the damage is created in a much shorter time and the observed effects are greater or equal to the real ones.

To perform this study, we used the hot line of the nuclear microprobe of the Pierre SÜE laboratory at CEA Saclay, France, where experiments with irradiated nuclear fuel are possible. It was thus possible to measure the xenon concentration using proton induced X-ray emission (PIXE) and to irradiate samples with an α beam in the same experimental set-up. The analysis of xenon and neodymium PIXE measurements was first carried out by comparison with the electron probe micro analysis (EPMA) results. The sample was then irradiated with a beam on some well-defined area and the xenon concentration was checked after irradiation.

2. Experimental aspects

2.1. Nuclear microprobe

The nuclear microprobe is an efficient tool for the measurement of the elemental composition of materials at the micron scale even at low concentration levels. The elementary composition is deduced from the detection and counting of various signals produced by the interaction of a high-energy light ion microbeam with the sample. This ion beam is produced and accelerated up to a few MeV by an electro-static accelerator, it is then mass-analysed by a dipole magnet and finally focused on the sample to the micron size by a set of quadrupolar electromagnetic lenses. Different kinds of interactions are produced during the slowing-down of the beam into the sample: PIXE is generated when the ions interact with inner-shell electrons; Rutherford back scattering (RBS) is produced when incoming ions are elastically scattered by the encountered nucleus; nuclear reaction analysis (NRA) occurs when an ion hits a nucleus, generally leading to particle or gamma emission. One major advantage of a Nuclear Microprobe is its versatility and the possibility of measuring a wide range of elements, varying from hydrogen to uranium.

The facility is equipped with two beam lines and one is exclusively dedicated to radioactive materials. The

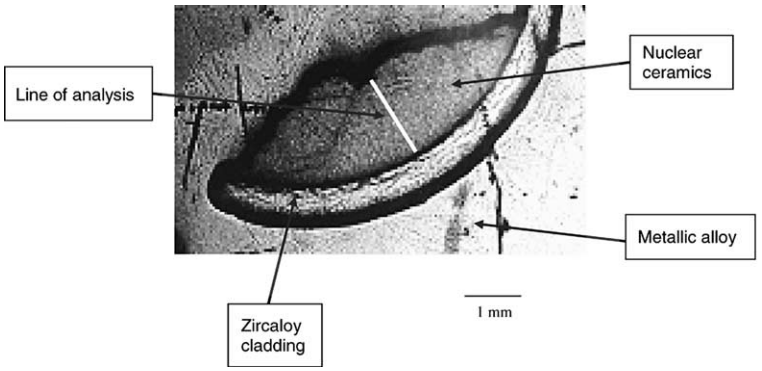

Fig. 1. Photograph of the sample. The slice of the fuel rod was polished so that only a small amount of nuclear ceramic remains in the metallic embedding. The red line indicates the location where most of the measurements were performed.

environment of the reaction chamber is similar to those used in hot electron microprobes [15].

2.2. Sample

The UO_2 sample, with an initial ^{235}U enrichment of 4.5%, is taken from a PWR fuel rod with Zircaloy cladding, irradiated in an EDF power plant for five cycles with an average burn-up of 57.6 GWd/tU. Its mean linear heat generation rate was 220, 270, 230, 190 and 170 $W\,cm^{-1}$ from first to fifth cycle. As fabricated, the pellets which are 8.19 mm in diameter, and 13.7 mm long exhibit a 10.45 density with a total porosity of 4.4%. The grain size varies from 12.2 μm at the pellet edge to 10.2 μm at the pellet centre.

Sampling was done at 320 mm from the bottom of the fissile column. Local burn-up is there about 62 GWd/tU. The slice obtained was polished up to a surface roughness of about 1 μm. The sample was embedded in a metallic alloy with a low melting point, as required for EPMA. To lower gamma irradiation in the experimental set-up, thinning was also performed in order to reduce the sample volume. Because of this special polishing, only a peripheral part of the slice containing nuclear ceramic was retained. A photograph of this sample is given in Fig. 1.

2.3. α irradiation conditions

The energy of the α beam was chosen so that the induced damage could be measured. The xenon concentration is indeed determined by measuring the intensity of its X-ray Lα line (4.110 keV) generated by proton irradiation. The absorption coefficient of this line in UO_2 is equal to 1.2 μm^{-1}. The transmitted signal of the line is represented as a function of the depth under the UO_2 sample surface in Fig. 2. From this figure it is clear that the xenon located at depth higher than 1 μm can not be correctly detected using the Xe Lα line.

In irradiated fuel, α particles have an average energy of 5.5 MeV and their penetration depth in UO_2 is more than 10 μm. However the Frenkel defects, which are likely to interact with fission products, are only created

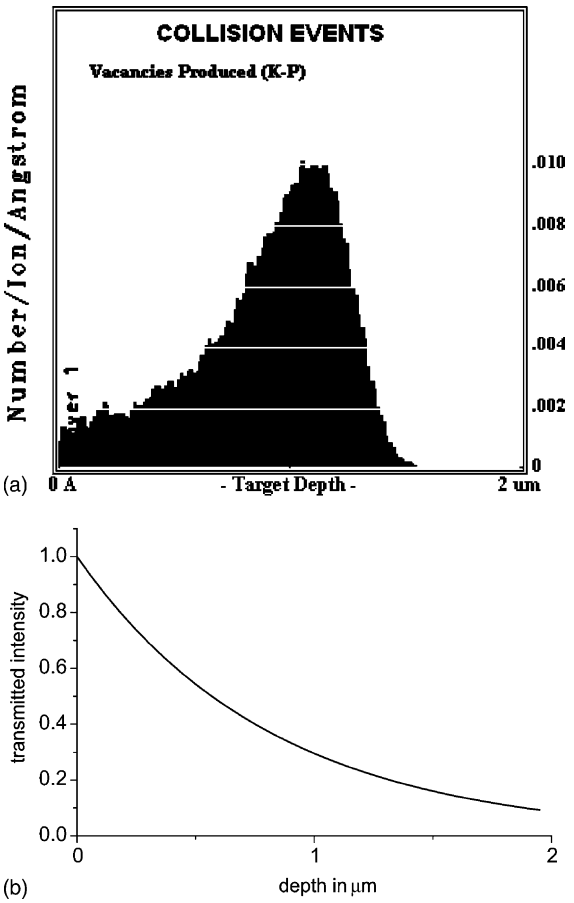

Fig. 2. Comparison between (a) damage produced by α irradiation (SRIM 2003 calculation) and (b) transmision yield of the Xe Lα line as a function of depth in UO_2.

at the end of the track. So if a 5.5 MeV beam was used in our α irradiation experiment, the damage created would lie at a depth where it would not be possible to measure the xenon concentration. That is why the α beam energy chosen was 500 keV in order to have an mean irradiation depth of 1.1 μm, large enough to avoid surface effects and small enough to reduce the X-ray attenuation for xenon Lα line. The distribution of the damage created by the α irradiation was calculated with SRIM 2003 and is presented in Fig. 2. The difference between the energy of the α beam in storage conditions and in our experiment only changes the length in which α particles are stopped by electronic interactions, but not by the creation of Frenkel pairs which occurs at the end of the track.

The α implanted dose was determined by measuring the electrical charge deposited in the sample by the primary beam. The accuracy of this measurement is warranted by the fact that UO_2 is an electrical semiconductor and by the fact that the sample voltage is 90 V lower than the voltage of the vacuum chamber which forces the secondary electrons, created by the interaction of the primary beam with sample, to come back to the sample. The α dose was monitored in order to lead to a concentration of α implantation tracks equivalent to the one that would be created in storage conditions. Because α self-irradiation in storage conditions is isotropic, the concentration of α tracks is equal to the concentration of created He and the concentration calculated for 300 years of storage in a MOX $D = 2 \times 10^{20}$ at./cm^3 was taken as a reference. In our experiment the α irradiation was not isotropic and the track concentration is calculated as the implanted dose in at./cm^2 divided by the He mean implantation depth.

The sample was irradiated on squares with a surface of 120×120 μm^2 by scanning a 30×30 μm^2 beam. In these squares the dose is maximum in a central area of 60×60 μm^2 which receives 41% of the total dose. Taking into account an approximate implantation depth of 1 μm, the concentration of α tracks is equal to $D = 20 \times 10^{20}$ tracks/cm^3 in the central area when implanting 7.2×10^{12} He^+ ions in this area, which represents a charge of 1.16 μC corresponding to a total implanted charge of 2.7 μC.

The squares relative positions and their location on the sample are schematically represented in Fig. 3. Squares 1 to 4 were aligned on the line of analysis shown in Fig. 1, their α track concentrations at the centre was close to D/100, D/10, D and 10 D for square 1, 2, 3 and 4 respectively. The distance between each square is 100 μm. The squares were more than 500 μm apart from the pellet edge in order to avoid the xenon concentration fluctuation due to the rim effect. Square 5, on the contrary, was located near the pellet edge in order obtain information about rim behaviour under α irradiation, its α track concentration was close to 10 D.

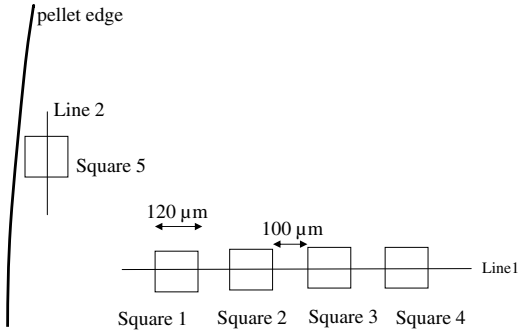

Fig. 3. Irradiation map: irradiated squares are labelled from 1 to 5. The line of PIXE analysis is labelled from 1 to 2. Square 1 is approximately 500 μm far from the pellet edge. The distance between the centres of the 120×120 μm^2 squares is 220 μm on line 1. PIXE measurements were performed on line 1 and 2.

2.4. PIXE measurements

Xenon and neodymium were measured by PIXE produced by a 3.6 MeV proton beam; the X-ray intensity was measured using a wave dispersive X-ray spectrometer. The spectra, collected by counting 100 s per point, are shown in Fig. 4. Their intensities are low and long acquisition times were required in order to extract them from the sample radioactive background.

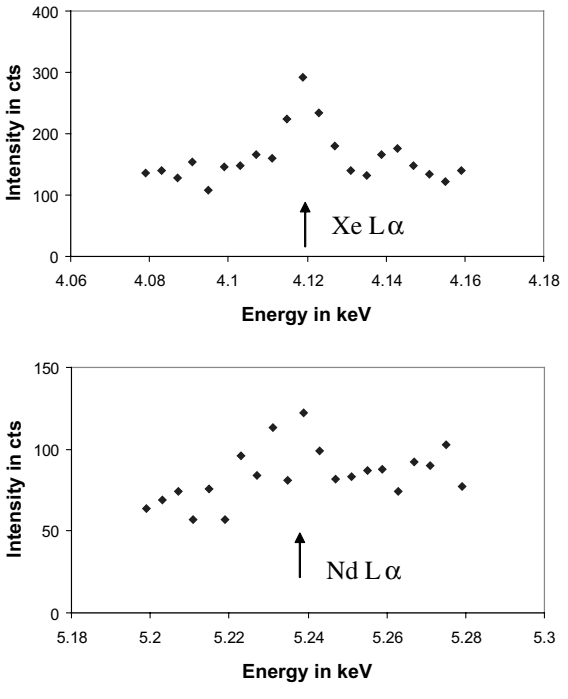

Fig. 4. Xenon and neodymium peaks measured by PIXE. The position of the Xe and Nd lines are indicated with an arrow. This position does not correspond exactly to the theoritical one because of the experimental errors.

For quantitative measurements, intensities at peak maximum and in background were measured. The background is due to the sample's own irradiation and to the proton irradiation. A normalised value of the peak intensity was calculated taking the proton dose into account. The accuracy of this measurement is correlated to the counting statistics with the Poisson's law.

The measurements were performed with 100 s counting per point, typical values are 360 counts for xenon with 140 counts of background which leads to a 15% accuracy. With a similar evaluation, the accuracy of the neodymium measurement is about 20%. The proton dose is estimated to a few % and it was not taken into account in this evaluation.

In order to obtain improved accuracy, several measurement points were averaged. In the following figures, about 10 points, which corresponds to a $\sim(100–150)\times 30$ μm^2 area, were averaged giving an improved accuracy of approximately 5%.

3. Results

3.1. Quantification of the PIXE measurements

In order to quantify the PIXE measurement and to check its reliability, xenon and neodymium were measured using this technique along a radius of the original slice of fuel rod along the line defined in Fig. 1. The results are presented in Fig. 5 compared with those performed using EPMA on a sample with a 61 GWd/tU local burn-up, located 800 mm from the bottom of the fissile column of the same fuel rod [5]. The PIXE curve was normalised to the one obtained by EPMA by adjusting the mean value of the xenon concentration of the PIXE curve to the mean value of the EPMA between 1000 and 2000 μm from the inner cladding. In this area, the UO_2 ceramics contains nearly no gas bubbles giving the best xenon concentration measurement.

The PIXE and EPMA curves are in rather good agreement when one first considers that they were not measured on the same sample and second, that the analysed surface is different for both techniques; the depth analysed by both techniques is approximately the same because it is limited by the absorption of xenon Lα line (see Section 2.3). EPMA measurements are performed on a 1 μm^2 surface, while the PIXE includes in this experiment 100×30 μm^2 which implies that the existence of gas bubbles under the sample surface induces some fluctuations in EPMA measurements which are smoothed in the PIXE curve.

3.2. Measurements on the α irradiated area

The measurements were performed as line-scans along 2 lines given in Fig. 3. The first line goes through square 1–4, line 2 through square 5. The xenon and neodymium concentrations measured along these lines are shown on Figs. 6 and 7.

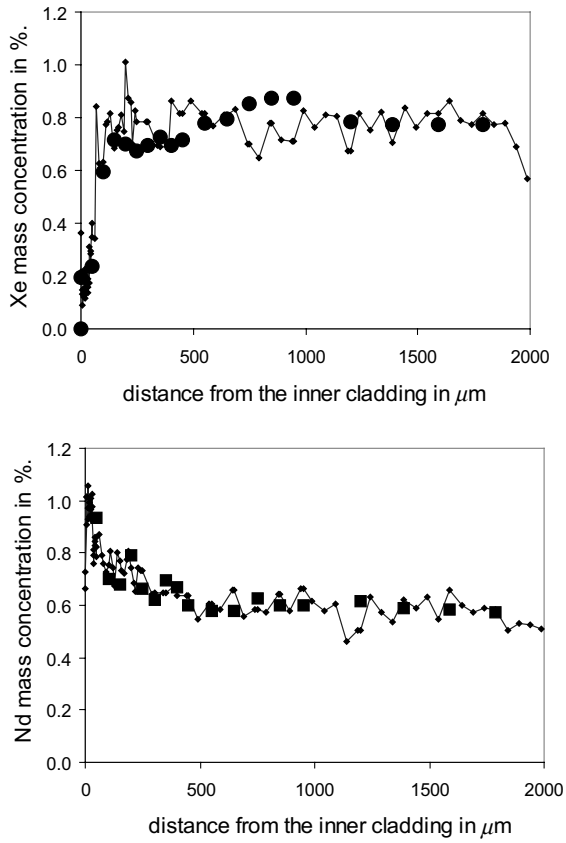

Fig. 5. Comparison of xenon and neodymium profiles as measured by PIXE (bold circle for Xe and bold square for Nd) and EPMA (line).

In irradiated fuel, neodymium is usually considered to stay where it has been created by fission, and it is unlikely to move under α irradiation. For this element, in Fig. 6 it can be seen that the points corresponding to an irradiated square are well aligned with the other points, showing no dispersion greater than twice the 5% estimated accuracy. The decrease of Neodymium concentration along line 2 is consistent with its evolution on Fig. 5 due to the decrease of the local burn-up. In Fig. 6, the xenon concentration is more or less constant whether the areas are α irradiated or un-irradiated. The concentration measured inside the α irradiated squares is nevertheless systematically less than in that non-irradiated area. In Fig. 7, xenon and neodymium concentration evolution in the rim area is emphasised. Within the 10% accuracy, no specific behaviour of xenon concentration is observed in the α irradiated squares compared to the un-irradiated areas.

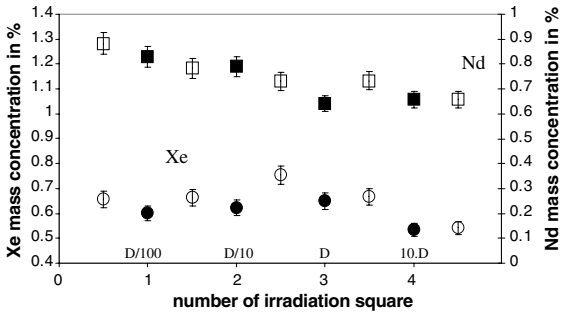

Fig. 6. Quantitative measurements of xenon (circle) and neodymium (square) mass concentration along line 1. The open symbols are the values averaged over 10 measurement points in an un-irradiated area (the area between squares). The filled symbols are the values averaged over 12 measurement points in an α-irradiated square.

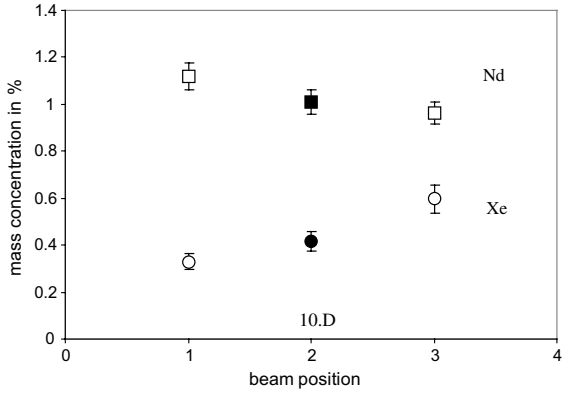

Fig. 7. Quantitative measurements of xenon (circle) and neodymium (square) mass concentration along line 2. Because line 2 is not strictly perpendicular to a pellet radius, a burn-up gradient leads to an increase of xenon signal and to a decrease of neodymium signal going from points 1 to 3. The beam positions 1 and 3 correspond to values averaged over 10 measurement points in an un-irradiated area on both sides of square 5. Beam position 2 corresponds to values averaged over 12 measurement points in α-irradiated square 5.

4. Discussion

In the introduction we stressed that either xenon athermal diffusion or rim formation might occur during interim storage. This two issues are discussed in the following. Xenon diffusion can be characterised very easily in our experiment because the analysed area lies near the sample surface. If xenon atoms diffused, they would indeed escape from the sample upon reaching the surface. From our experiments, we concluded that the xenon concentration kept the same value after α irradiation within an accuracy of 10%. The concentration measured inside the α irradiated square is systematically less than in that non-irradiated area, but this is probably not an effect due to α irradiation because it does not depend on the α implanted dose which varies over 4 decades between squares 1 and 4.

The 10% accuracy for the measurement of xenon concentration can be used as a detection limit to determine a maximum diffusion path of xenon in our experiments. A xenon depletion observed with PIXE is due to a migration of xenon out of the analysed volume. The xenon atoms could diffuse deeper under the surface or escape in the vacuum when reaching the sample surface. In our experiment no collision event exist at depth higher than 1.5 μm, so we consider only the migration of xenon to the surface. Thus the mean displacement of a xenon atom under α external irradiation determine the depth of a layer depleted of xenon at the surface after irradiation. Taking into account Fig. 2, one can calculate that a 0.1 μm depleted layer at the surface induces a decrease of xenon signal measured by PIXE of approximately 10%. Thus the diffusion path of xenon under α irradiation in our experimental conditions can be estimated not more than approximately 0.1 μm. No rim formation was observed in the α irradiated squares. The rim formation is indeed characterised by a sharp decrease in the xenon concentration measured with EPMA from around 0.8–0.2 wt% as evidenced in Fig. 5. However, the evolution of the xenon signal inside and outside the α irradiated square exhibits no such decrease. Moreover, inside square 5, which is located at the beginning of the rim area, the xenon concentration and the neodymium concentration behave in the same manner as they have no α irradiation. The rim formation is also characterised by an increase of the porosity. Using optical microscopy, it was determined that no additional porosity was created during the α irradiation. Only a slight change of colour was observed on the α irradiated square and this was attributed to the interaction of residual impurities with the α beam in the vacuum of the PIXE chamber. These results enable us to estimate that no major effect should be observed due to α irradiation for UO_2 and MOX fuels in storage conditions for the following reasons: In storage conditions, the behaviour of fission products in nuclear fuel might be detrimental if they escape from the ceramics. This escape is only possible if the fission products can diffuse over long distances in the intact ceramics or if they diffuse over shorter distances in powdered ceramics.

EPMA results revealed that only fission gases (xenon and krypton) and sometimes caesium have moved more than 1 μm from their birth location for fuel rod with a moderate heat power rate (200 W/cm). It is usually admitted that rare gases are the most mobile. So in the following we shall only consider these species. For fission gases, the diffusion process is well described. First the gas diffuses over a short distance to form nanobubbles, then some gas can diffuse to the grain

boundaries to form bubbles. These bubbles then grow and interconnect which allows the gas to escape from the ceramics. While the exact diffusion mechanisms are still a subject of debate, it is now clear that after irradiation a part of the remaining gas is located in bubbles on the grains boundaries in UO_2 and MOX fuel. Our results show that the xenon diffusion path under an α irradiation representative of storage conditions is less than 1 μm. Assuming that all the xenon contained in a 0.1 μm thick layer around a 10 μm diameter grain is released, it induces that a maximum of 6% of the grain gas inventory goes to the grain boundaries. The irradiated commercial MOX fuel can be considered as a mixture of high burn-up plutonium enriched phases diluted in a low burn-up UO_2 matrix. The concentration of xenon in the UO_2 matrix for a MOX fuel is lower than that of a UO_2 fuel with the same burn-up. Its behaviour should therefore not be different from the one observed in our experiment. The plutonium-enriched phases due to their high burn-up, are considered to be equivalent to the rim observed at the edge of the high burnup UO_2 pellets. The results obtained on square 5 prove that no modification of the xenon concentration is observed in the rim area of our sample. This result should also be true for the plutonium-enriched agglomerates in MOX fuel, although the local burnup is higher for a 3 cycle MOX agglomerate than for a 5 cycle UO_2 rim.

5. Conclusion

Our results revealed that no dramatic change in the xenon concentration of a highly irradiated UO_2 fuel occurred under α irradiation with a dose rate that is representative of storage conditions. From this result, it was deduced that for UO_2 and MOX fuel with standard burn-up in storage conditions, no more than 6% of the rare gases can diffuse to the grain boundaries under α particle irradiation.

This evaluation corresponds in fact to the detection limit of PIXE.

It proves that α irradiation has a little effect, if any, on the storage of nuclear fuel. The study of α auto-irradiation will now focus on the influence of atom recoil.

References

[1] C. Poinssot et al., Synthesis of the long term behaviour of the spent nuclear fuel, CEA report no. CEA-R-5958 (E), 2001.
[2] N. Chauvin et al., Synthesis on $MgAl_2O_4$, Technical report JRC-ITU- + TN-2002/39.
[3] H.J. Matzke, Radiat. Eff. 64 (1982) 3.
[4] W.J. Weber, Radiat. Eff. 83 (1984) 145.
[5] C.T. Walker, J. Nucl. Mater. 275 (1999) 56.
[6] N. Lozano, L. desgranges, D. Aymes, J.C. Niepce, J. Nucl. Mater. 257 (1998) 78.
[7] K. Nogita, K. Une, J. Nucl. Mater. 226 (1995) 302.
[8] J. Rest, G.L. Hofmann, J. Nucl. Mater. 277 (2000) 231.
[9] L.E. Thomas, C.E. Beyer, L.A. Charlot, J. Nucl. Mater. 188 (1992) 80.
[10] J. Spino, D. Baron, M. Coquerelle, A.D. Stalios, J. Nucl. Mater. 256 (1998) 189.
[11] A.J. Mill, CEGB Berkeley Nuclear Lab. TPRD/B/0219/N83.
[12] W.J. Weber, R.C. Ewing, C.R.A. Catlow, T. Diaz de la Rubia, L.W. Hobbs, C. Kinoshita, H. Matzke, A.T. Motta, M. Nastasi, E.K.H. Salje, J. Mater. Res. 13 (1998) 1434.
[13] M. Pelletier, J.P. Piron, J. Pavageau, NEA Seminar Proceedings on Fission gas behaviour in Water Reactor fuel held in Cadarache (France) 26–29 September 2000, p. 311.
[14] Hj. Matzke, Radiat. Eff. 64 (1982) 3.
[15] H. Khodja et al., ICNMTA 2000, Bordeaux, France, September 2000.